LECTURE NOTES
OF
SUBNUCLEAR PHYSICS

Collection of the lectures notes of professor Donatella Lucchesi.

Edited By

Ardino Rocco

Academic year 2019-2020

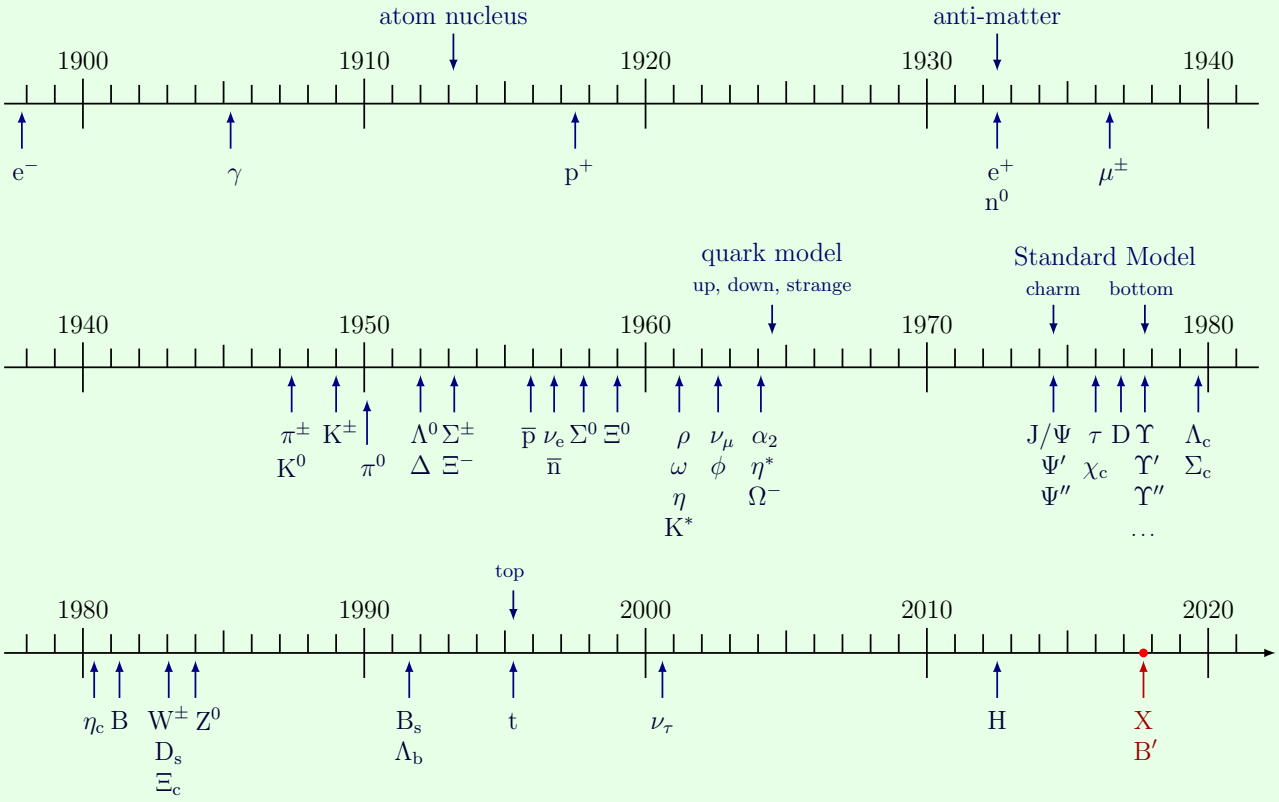

Contents

Course structure and program

Lecture 1.
Tuesday 10^{th} March, 2020.
Compiled: Friday 27^{th} March, 2020.
Prof. Lucchesi

Informations

Suggested books:

- *Concepts of Elementary Particle Physics*, Michael E. Peskin.
  It has a very good experimental approach, with theoretical concepts explained as well.
- Any other book where the same topics are presented is fine. For example, the book of Alessandro Bettini.

Exam modalities: the exam is slitted into two parts. These are:

- **Written exercises**.
  The idea is to prepare two partial tests: one will take place almost at the middle of the course, one at the end. For each chapter of the reference book there are several exercises that are useful for the comprehension of the topics of the course.
- **Oral discussion**.
  It will be focused on a single topic and it will take place after the written part.

The final evaluation will be a weighted mean of the two written exercises and of the oral discussion.
Remeber to subscribe to the Facebook group *Subnuclear Physics at DFA* for further informations and for infos on seminars of particle physics.

Course Program

- **Introduction and recap**
- **Tools for calculation**.
  In order to understand all the following topics, we need some mathematical tools (that we already have but the way we are going to use them is different from the use we did in theoretical physics course). They are needed to evaluate the physical phenomena we are going to discuss.
- **Detectors for particle physics experiments**.
  They are needed to perform measurements, so it is important to acquire a certain knowledge on them. For example, in order to choose why a detector is better than another one for a certain task and to set up a particle physics experiment. This part is not well described in the reference book, so we will use other books for this purpose.
- **Cross section of $e^+e^- \longrightarrow \mu^+\mu^-$ and $e^+e^- \longrightarrow hh$.**
  The former is a very simple process and it is important for the study of many other processes. The ladder will be important to understand the basis of QCD.

- **Strong interactions**:
  - ▷ **Deep inelastic scattering**
  - ▷ **Gluon**
  - ▷ **QCD**
  - ▷ **Partons and jets**
- **Electroweak interactions** (This part and the part on strong interactions sum up into the discussion on Standard Model):
  - ▷ **V-A Weak theory**.
    It is the theory at the base of electroweak interaction, which we will build up.
  - ▷ **Gauge theory and symmetry breaking**.
    This part will be discussed not so deeply since it was treated during the course of *Theoretical Physics of Fundamental Interactions*.
  - ▷ W **and** Z^0 **bosons**.
    The most important items and measurements will be presented.
  - ▷ **Cabibbo theory and CKM**.
    This part is needed in order to put the hadrons, in particular the quarks, into the electroweak theory. However, it will not be discussed deeply since it was presented during the bachelor course *Introduction to Nuclear and Subnuclear Physics*.
  - ▷ **CP violation, the B meson system**.
    It will be a more experimental discussion.
- **New Physics** (we will try to give an answer to how we can go beyond the description given by Standard Model, in fact there are phenomena that are still not explained by this theory):
  - ▷ **Neutrino and Standard Model**
  - ▷ **Higgs properties**

Chapter 1

Introduction and Recap

1.1 Basic knowledge

Relativistic wave equations

Relativistic quantum field theory is necessary to describe quantitatively elementary particle interactions. Its description is not part of this course, so we will use it in simple cases and only when necessary.
It is assumed the following knowledge:

- Klein-Gordon equation (for boson fields):

$$\left(\frac{\partial^2}{\partial t^2} - \boldsymbol{\nabla}^2 + m^2\right)\psi(t, \vec{\mathbf{x}}) = 0 \tag{1.1}$$

- Dirac equation (Klein-Gordon can't give a description for fermion fields):

$$\left(i\gamma_\mu \frac{\partial}{\partial x_\mu} - m\right)\psi(t, \vec{\mathbf{x}}) = 0 \tag{1.2}$$

  with $\psi = (\psi_1, \psi_2, \psi_3, \psi_4)$

- Basic concepts of fields and particles
- Basic concepts of Feynman diagrams

Natural Units

During the course we will use the natural units, therefore:

$$\hbar = c = 1 \tag{1.3}$$

Considering that:

$$1 \text{ eV} = 1.6 \cdot 10^{-19} \text{ J}$$
$$c = 3 \cdot 10^8 \text{ m/s}$$

we have:

$$1 \frac{\text{eV}}{c^2} = 1.78 \cdot 10^{-36} \text{ Kg}$$

Since $E^2 = p^2c^2 + m^2c^4$, it is convenient to measure p in GeV/c and m in GeV/c^2. For example the electron mass $m_e = 0.91 \cdot 10^{-27}$ g corresponds to $m_e = 0.51$ MeV/c^2. It is also useful to remember that $\hbar c = 197$ MeVfm.
An interesting quantity to consider in natural units is the strength of the electric charge of the electron or proton. By taking into account the potential $V(r) = \frac{e^2}{4\pi\varepsilon_0 r}$, the radius r in natural units has a dimension of Energy^{-1}. By this way it forces the following relation:

$$\alpha \equiv \frac{e^2}{4\pi\varepsilon_0\hbar c} = \frac{1}{137.036} \tag{1.4}$$

namely, the **fine structure constant**.

Symmetries

They are the corner stones of particle physics. The most important ones for our studies are the **space-time symmetries**, which can be classified into:

- Continuous symmetries:
  - ▷ Translation in time. The generator of the group of time translations is the operator H, namely the Hamiltonian, which is linked to the energy quantity.
  - ▷ Translation in space. The generator of the group of space translations is the operator $\vec{\mathbf{p}}$, namely the momentum.
  - ▷ Rotations. In this case, the generator of the group of this kind of transformations is the angular momentum $\vec{\mathbf{L}}$.

  If a system is invariant under one of these transformations, the corresponding generator, so H, $\vec{\mathbf{p}}$ or $\vec{\mathbf{L}}$, is conserved.

- Discrete symmetries:
  - ▷ Parity P:

    $$x^\mu = (x^0, \vec{\mathbf{x}}) \xrightarrow{P} (x^0, -\vec{\mathbf{x}}) \tag{1.5}$$

    Fermions have half-integer spin and angular momentum conservation requires their production in pairs. We can define therefore just relative parity. By convention, the proton p has parity equal to $+1$. The parity of the other fermions is given in relation to the parity of the proton.

    Parity of bosons can be defined without ambiguity since they are not necessarily producted in pairs.

    Parity of a fermion and its antiparticle (i.e. an antifermion) are opposite, while parity of a boson and its anti-boson are equal.

    Moreover, the parity of the positron is equal to -1. Quarks have parity equal to $+1$, leptons have parity equal to $+1$. Their antiparticles have parity equal to -1.

    Lastly, parity of a photon is equal to -1.
  - ▷ Time Reversal T:

    $$x^\mu = (x^0, \vec{\mathbf{x}}) \xrightarrow{T} (-x^0, \vec{\mathbf{x}}) \tag{1.6}$$

▷ Charge Conjugation C:

$$\text{Particle} \xleftrightarrow{C} \text{Antiparticle} \tag{1.7}$$

It is needed in order to restore a complete symmetry under the exchange of a particle with its antiparticle. A photon has -1 eigenvalue under C, which means: $C\,|\gamma\rangle = -\,|\gamma\rangle$.
Fermion-antifermion have opposite intrinsic parity and for non elementary particles the total angular momentum has to be considered, in fact the C parity goes like $(-1)^{\ell}$ or $(-1)^{\ell+1}$ (depending on the intrinsic parity).

Fundamental constituents of the matter

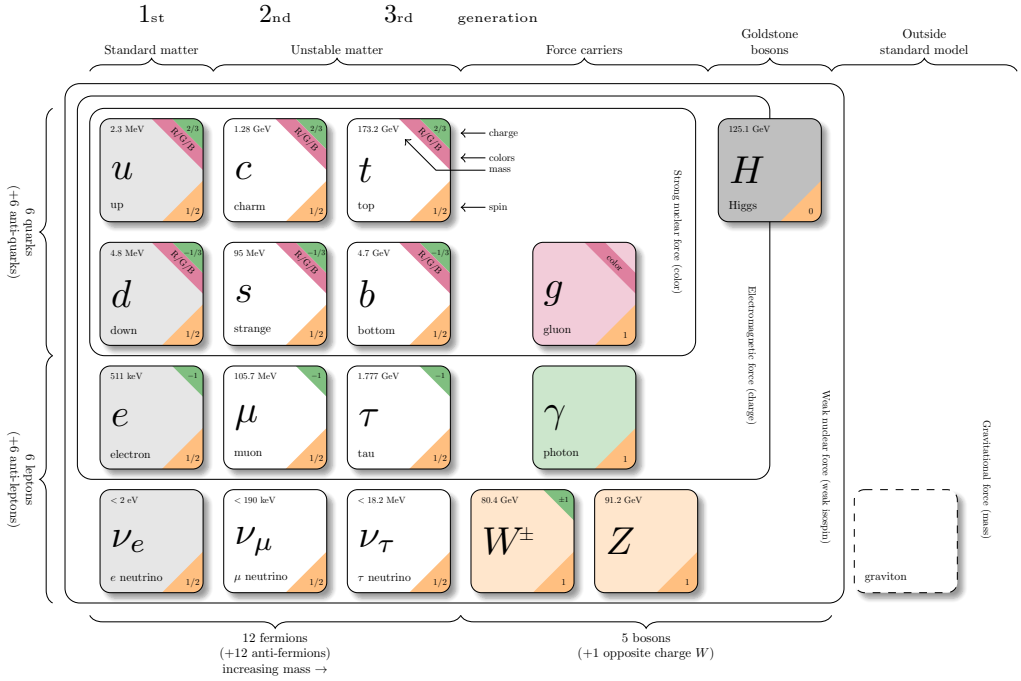

Figure 1.1: Standard Model particles.

Lecture 2.
Wednesday 11th March, 2020.
Compiled: Friday 27th March, 2020.
Prof. Lucchesi

1.2 Hydrogen atom and Positronium

We are going to study the already known system of the hydrogen atom, and compare it to the system of positronium. More in detail, our goal is to understand the e^+e^- bound state and the possible application of this model to the description of other systems. Therefore, we start from the hydrogen atom since it has some characteristics in common with the positronium.
In QM Physics, this bound state is really similar to the hydrogen atom. The assumptions for this one in the non relativistic limit are that the mass of the proton is much bigger than the mass of the electron ($m_p >> n_e$) and the potential is given by:

$$V(r) = -\frac{e^2}{4\pi r} = -\frac{\alpha}{r} \tag{1.8}$$

From this potential, by solving the Schrödinger equation, we get the bound state energies:

$$E = -\frac{R_y}{n^2} \tag{1.9}$$

R_y is known as **Rydberg energy**, whose expression reads:

$$R_y = \frac{1}{2}\frac{me^4}{(4\pi)^2} = 12.6 \text{ eV} \tag{1.10}$$

$$R_y = \frac{1}{2}\alpha^2 m_p \qquad \text{In natural units} \tag{1.11}$$

The bound states of hydrogen are arranged in levels associated with integers $n = 1, 2, 3, \ldots$. Each level contains the orbital angular momentum states:

$$\begin{aligned} \ell &= 0, 1, \ldots, n-1 \\ m &= -\ell, \ldots, \ell \end{aligned} \tag{1.12}$$

The orbital wavefunctions are the spherical harmonics $Y_{\ell m}(\theta, \varphi)$, which are even under spatial reflection for even ℓ and odd for odd ℓ. Then, under P, these states transform as:

$$P\,|n\ell m\rangle = (-1)^\ell\,|n\ell m\rangle \tag{1.13}$$

However, with these assumptions, we are not considering that the real hydrogen atom has more structure. In fact, we are negleting that the electron is a particle with intrinsic spin and we have to take into account also this quantity. In a more technical way, we have to add the contribution of the spin-orbit interaction (fine splitting), which is proportional to the scalar product $\vec{\mathbf{L}}\cdot\vec{\mathbf{S}}$. Concerning the Hamiltonian of this contribution, it is given by:

$$\Delta H = \frac{g-1}{2}\frac{\alpha}{m^2 r^3}\vec{\mathbf{L}}\cdot\vec{\mathbf{S}} \tag{1.14}$$

The sign is such that the state with $\vec{\mathbf{L}}$ and $\vec{\mathbf{S}}$ opposite in sign has lower energy. Moreover, it may be useful to express the operator $\vec{\mathbf{L}}\cdot\vec{\mathbf{S}}$ in terms of J^2, L^2, S^2:

$$\vec{\mathbf{J}} = \vec{\mathbf{L}} + \vec{\mathbf{S}} \Longrightarrow \vec{\mathbf{L}}\cdot\vec{\mathbf{S}} = \frac{1}{2}\left(\left(\vec{\mathbf{L}}+\vec{\mathbf{S}}\right)^2 - L^2 - S^2\right) = \frac{1}{2}\left(J^2 - L^2 - S^2\right) \tag{1.15}$$

By this way it is straightforward to diagonalize the operator $\vec{\mathbf{L}}\cdot\vec{\mathbf{S}}$. At the end we get the order of magnitude of the spin-orbit interaction:

$$\left\langle \frac{\alpha}{m^2 r^3} \right\rangle \sim \frac{\alpha}{m^2 a_0^3} \sim \alpha^4 m \sim \alpha^2 R_y \tag{1.16}$$

Thus, this effect is a factor of 10^{-4} smaller than the splitting of the principal levels of hydrogen.
Another contribution that we have to add is the spin-spin interaction (hyperfine splitting) between electron and proton, which leads to the addition of another term into the total Hamiltonian. The magnetic moments of the proton and the electron interact, with the ground state favoring the configuration in which the two spins are opposite. Therefore:

$$\Delta H = C\vec{\mathbf{S}}_p \cdot \vec{\mathbf{S}}_e \tag{1.17}$$

where the C constant depends on the electron wavefunction.
Hence, we have several levels for the spin states. For example, the 1S state of hydrogen is split into two levels, corresponding to the total spin:

$$\vec{\mathbf{J}} = \vec{\mathbf{S}}_p + \vec{\mathbf{S}}_e \tag{1.18}$$

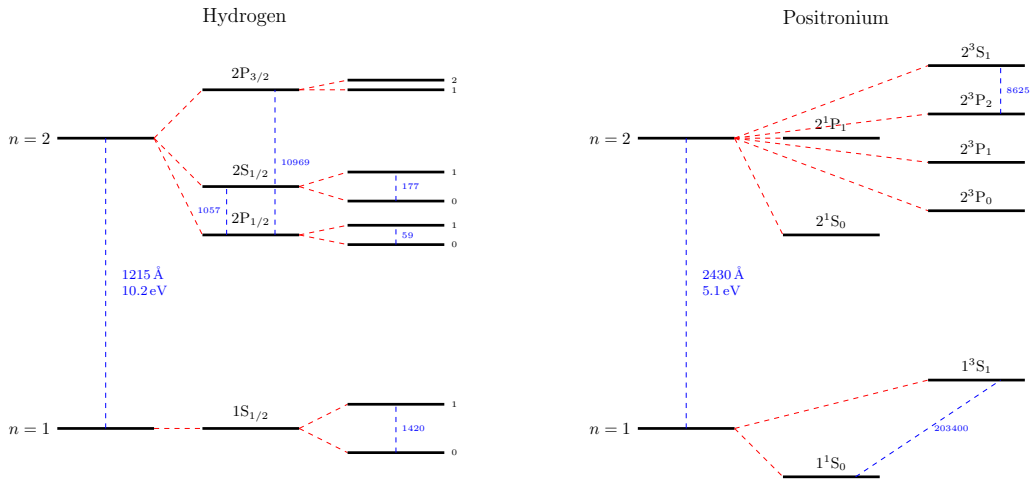

Figure 1.2: Comparison of the 1S, 2S, and 2P energy levels of hydrogen atom and positronium.

The possibilities we have are 2: $J = 0$ and $J = 1$, depending on how the two spin states of proton and electron combine. The projection on the z-axis gives 3 possibilities: $J_z = 1, 0, -1$ (corresponding to $|\uparrow\uparrow\rangle$, $\frac{1}{\sqrt{2}}(|\downarrow\uparrow\rangle + |\uparrow\downarrow\rangle)$, $|\downarrow\downarrow\rangle$).
Now the possibility that we have to evaluate is that e^+e^- forms bounded states. In fact, the same ideas can be applied to a particle-antiparticle system and the simplest case is the positronium.
It is relatively easy to make positronium. In colliders, when working with a beam of positrons which enter in the matter, they can pick up an electron and form a bounded state of positronium, so this the starting point of the idea. All the considerations applied to the case of hydrogen atom can be applied to the positronium case as well. All the calculations are omitted. The first consideration is that here we can't apply the approximation $m_p >> m_e$, in fact the two particles here have the same mass. The solution for this two-body problem is to use the reduced mass μ, namely:

$$\mu = \frac{m_1 m_2}{m_1 + m_2} = \frac{m_e}{2} \tag{1.19}$$

At the end of all the calculations we won't do, we get that the hyperfine splitting contribution is approximately of the same of order of magnitude of the fine splitting and both are of the order $\alpha^4 m_e$.
Now we have to classify the eigenstates under parity and charge conjugation of the positronium. Let's consider first P. The intrinsic parity of the electron is $P_{e^-} = +1$, of the positron $P_{e^+} = -1$. So the parity of a single particle goes like $P = (-1)^\ell$ and the overall parity goes like $P = (-1)^{\ell+1}$.
For C, we must account three effects:

- C converts the electron to the positron and the positron to the electron. The electron and positron are fermions, and so, when we put the electron and positron back into their original order in the wavefunction, we get a factor -1.

- Reversal of the coordinate in the orbital wavefunction gives a factor $(-1)^\ell$.

- Finally, the electron and positron spins are interchanged. The $S = 1$ state is

symmetric in spin, but the $S = 0$ state is antisymmetric.

$$S = 0 \longrightarrow \frac{1}{2}(|\uparrow\downarrow\rangle - |\downarrow\uparrow\rangle)$$
$$S = 1 \longrightarrow |\uparrow\uparrow\rangle \qquad \frac{1}{2}(|\uparrow\downarrow\rangle + |\downarrow\uparrow\rangle) \qquad |\downarrow\uparrow\rangle$$

and so gives another factor (-1).

In all, the positronium states have C:

$$C = (-1)^{\ell+1} \cdot \begin{cases} 1 & S = 1 \\ -1 & S = 0 \end{cases} \tag{1.20}$$

and what we get is the J^{PC} scheme. The low-lying states of the positronium spectrum then have the J^{PC} values as in Figure 1.3.

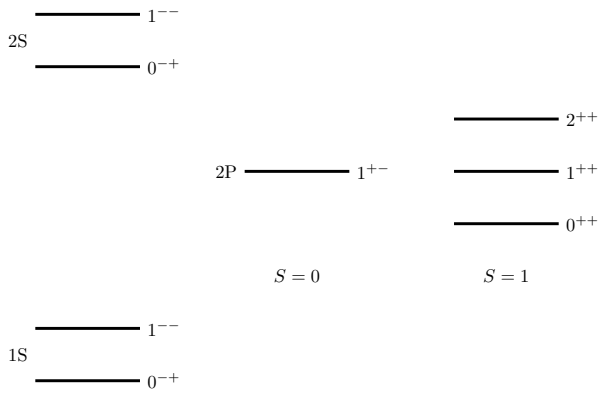

Figure 1.3: J^{PC} scheme. The 2P states 0^{++}, 1^{++} and 2^{++} arise from coupling the $L = 1$ orbital angular momentum to the $S = 1$ total spin angular momentum.

We know that electron and positron annhilate each other, so this state decays into something. The rules are E and $\vec{\mathbf{P}}$ conservation. It can't decay into a single photon since the momentum is not conserved. Recall that:

$$C\,|\gamma\rangle = -1 \Longrightarrow C\,|n\gamma\rangle = (-1)^n \tag{1.21}$$

If we are looking for the two photon decay (so positive conjugation) of the positronium, the only possible state is the one with $S = 0$. If we are looking for a three photon decay (so negative conjugation), the only possible state is the one with $S = 1$. This kind of decay has been verified experimentally.
Positronium with state $S = 0$ is also known as **para-positronium**. If the state is $S = 1$, it is also known as **ortho-positronium**. Their medium lifes are:

$$\frac{1}{\tau_{\mathrm{p}}} = \frac{1}{2}\alpha^5 m \qquad \tau_{\mathrm{p}} = 1.2 \cdot 10^{-10}\ \mathrm{s} \tag{1.22}$$
$$\frac{1}{\tau_{\mathrm{o}}} = \frac{2}{9\pi}(\pi^2 - 9)\alpha^6 m \qquad \tau_{\mathrm{o}} = 1.4 \cdot 10^{-7}\ \mathrm{s} \tag{1.23}$$

So, when we emit positrons into a gas, $\frac{1}{4}$ of the states decays quickly in τ_{p}, while $\frac{3}{4}$ of the states decays slower in τ_{o}. It is a strange result, but experiment verifi es it (Berko and Pendleton, 1980).

1.3 Static Quark Model

A beautifully simple way to create any particle, together with its antiparticle, is to annihilate electrons and positrons at high energy. The annihilation results in a short-lived excited state of electromagnetic fi
elds. This state can then re-materialize into any particle-antiparticle pair that couples to electromagnetism and has a total mass less than the total energy of the annihilating e^+e^- system.

1.3.1 Light quarks: charm and beauty

By this way, the importance of the positronium state is clear. Moreover, it is linked to the discovery of quark charm and beauty.
Their discovery takes place in 1974 at SPEAR experiment, where by studying the process $e^+e^- \longrightarrow hh, \mu^+\mu^-,\ e^+e^-$, an enormous, very narrow, resonance at about 3.1 GeV was discovered. This resonance would correspond to a new strongly interacting particle.
When they announced this discovery, they learned that the group of Samuel Ting, working at Brookhaven National Laboratory in Upton, New York, had also observed this new particle. Ting's group had studied the reaction $pp \longrightarrow e^+e^- + X$, where the particles X are not observed.
This never observed particle is now called the J/ψ. A few weeks later, the SPEAR group discovered a second narrow resonance at 3686 MeV, the ψ'.
Another group of narrow resonances is found in e^+e^- annihilation at higher energy. The lightest state of this family, called Υ, has a mass of 9600 MeV. It was discovered by the group of Leon Lederman in the reaction $pp \longrightarrow \mu^+\mu^- + X$ at the Fermilab proton accelerator.
Concerning the J/ψ, this particle is given by a quark doublet $c\bar{c}$ called **charmonium**. If this state exists, we will see phenomena like the ones observed with positronium. In the process $e^+e^- \longrightarrow hh$, the highest rate reactions are those in which e^+e^- pair is annihilated by the electromagnetic current $\vec{\mathbf{j}} = \bar{\psi}\vec{\gamma}\psi$ through the matrix element:

$$\langle 0 | \vec{\mathbf{J}}(x) \left| e^+e^- \right\rangle \tag{1.24}$$

The current has spin 1, $P = -1$, and $C = -1$. These must also be properties of the annihilating e^+e^- state, and of the new state that is produced. So, all of the ψ and Υ states must have $J^{PC} = 1^{--}$.
The current creates or annihilates a particle and antiparticle at a point in space. So, if these particles are particle-antiparticle bound states, the wavefunctions in these bound states must be nonzero at the origin. Most probably, they would be the 1S, 2S, etc. bound states of a potential problem. If this guess is correct, the states with higher L must also exist. They might be produced in radiative decays of the ψ and Υ states. Indeed, there is an experimental evidence, with a pattern of states as in Figure 1.4.
Remarkably, this reproduces exactly the pattern of the lowest-energy states of positronium and makes even more clear that the analogy to positronium is precise. In the case of the ψ family, the fermion is called the charm quark (c); this quark has a mass of about 1.8 GeV. In the case of the Υ family, the fermion is called the bottom quark (b); this quark has a mass of about 5 GeV.

Lecture 3.
Tuesday 17th March, 2020.
Compiled: Friday 27th March, 2020.
Prof. Lucchesi

1.3.2 Light mesons

Now we can go back to the π mesons and other relatively light hadrons. πs are the strongly interacting particles and there are three π mesons: π^0, π^+ and π^-.

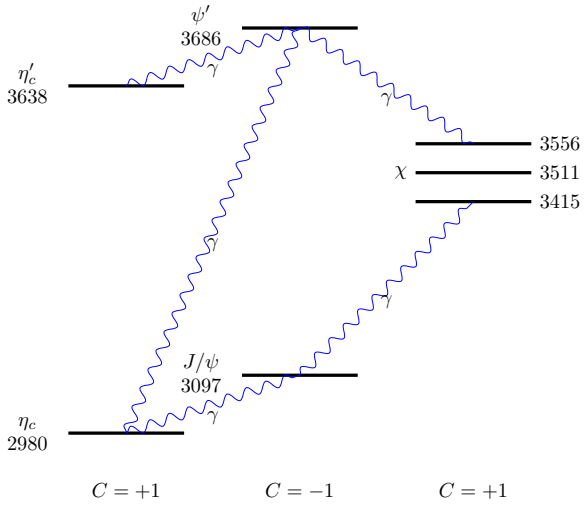

Figure 1.4: Pattern of states for the charmonium.

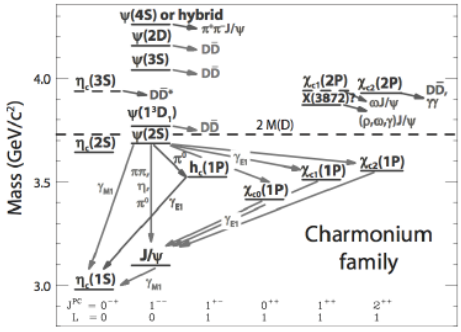

Figure 1.5: Observed states and transitions of the J/ψ system.

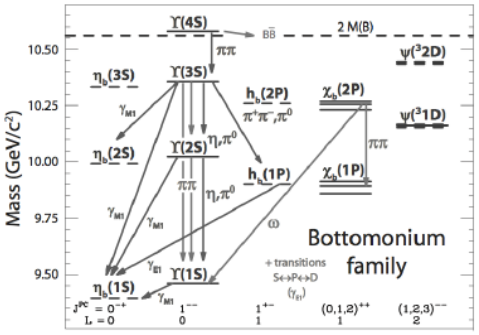

Figure 1.6: Observed states and transitions of the Υ system.

Their history is the beginning of modern particle physics and they were discovered in 1947, when Lattes, Occhialini and Powell demonstrated the existence of $\pi^{\pm}$ through $\pi^{\pm} \longrightarrow \mu^{\pm} + \nu$.
By detailed study of their interactions, it was determined that the π mesons also had $J^P = 0^-$. The π^0 decays to 2 photons, so it is $C = +1$. All of this is consistent with the interpretation of the pions as spin-$\frac{1}{2}$ fermion-antifermion bound states.
There are 9 relatively light 0^- hadrons, also known as **pseudoscalar mesons**, and 9 somewhat heavier 1^- hadrons, called the **vector mesons**, presented in Figure 1.7. The K and K^* states are not produced singly in strong interactions. They are only produced together with one another, or with special excited states of the proton. For example, we see the reactions:

$$\pi^- p \longrightarrow nK^+K^-$$
$$\pi^- p \longrightarrow \Lambda^0 K^0$$

where Λ^0 is a heavy excited state of the proton, but we don't see the reaction:

$$\pi^- p \longrightarrow nK^0$$

For this reason, the K mesons and the Λ^0 baryon became known as the strange particles.
As a consequence of this discovery, a new quantum number, the **strangeness**, was introduced to describe the production and decay processes. It was found that the

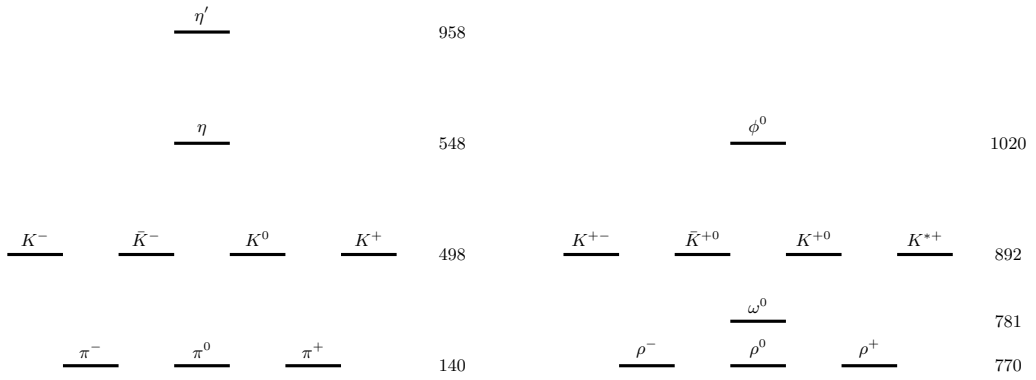

Figure 1.7: Light mesons summary. On the left there are the pseudoscalar mesons, on the right the vector mesons. The numbers given are the masses of the particles in MeV.

rules for K and K^* production can be expressed simply by saying that the strong interaction preserves the strangeness, with K^0, K^+, K^{*0} and K^{*+} having strangeness $S = -1$, their antiparticles having $S = +1$, and the Λ^0 having $S = +1$. Moreover, with the introduction of strangeness, a new kind of quark was introduced in the theories, namely the strange quark s. States with strangeness $+1$ will be assigned one s quark, and states with strangeness -1 will have one $\bar{s}$ antiquark.

1.4 Leptons

The leptons are fundamental particles, divided in several classes. We have:

- **Electron** e.
  It was discovered by J.J. Thomson in 1897 while studying the properties of cathode rays.

- **Muon** μ.
  It was discovered by Carl D. Anderson and Seth Neddermeyer in 1936 as component of the cosmic rays. At the beginning it was thought to be the Yukawa particle, the mediator of the strong force. Then Conversi, Pancini and Piccioni gave a proof that it does not interact strongly.

- **Tauon** τ.
  It was discovered by a group led by Martin Perl at Stanford Linear Accelerator Center. They used e^+e^- collisions with final states events $e\mu$.

- **Neutrino** ν.
  Neutrino hypothesis was formulated by Pauli to explain the β-decay. It was discovered by Clyde Cowan and Fred Reines in the 1953. We don't know if mass is given to neutrinos through the same mechanism (Higgs mechanism) for the other particles or if there is something that does it that we still don't know.

Chapter 2

Tools for calculations

To compare the results of elementary particle experiments to proposed theories of the fundamental forces, we must think carefully about what quantities we can compute and measure. We cannot directly measure the force that one elementary particle exerts on another. Most of our information about the subnuclear forces is obtained from scattering experiments or from observations of particle decay.
In scattering experiments, the basic measureable quantity is called the **differential cross section**. In particle decay, the basic measureable quantity is called the **partial width**.

2.1 Observables in experimental particle physics

The basic observable quantity associated with a decaying particle is the **rate of decay**. In quantum mechanics, an unstable particle A decays with the same probability in each unit of time. The probability of survival to time t then obeys the differential equation:

$$\frac{\mathrm{d}P(t)}{\mathrm{d}t} = -\frac{P}{\tau_A} \overset{\text{solution}}{\Longrightarrow} P(t) = P_0 e^{-\frac{t}{\tau_A}} \tag{2.1}$$

The decay rate τ_A^{-1} is also called the **total width** Γ_A of the state A. Its dimension is 1/sec, equivalent to GeV up to factors of $\hbar$ and c.

$$\tau_A = \frac{1}{\Gamma_A} \qquad \Gamma_A = \text{Total width of the state } A \tag{2.2}$$

If there are multiple decay processes like $A \longrightarrow f$, each process has a rate $\Gamma(A \longrightarrow f)$, namely the **partial width**. Thus, the total decay rate is given by:

$$\Gamma_A = \sum_f \Gamma(A \longrightarrow f) \tag{2.3}$$

Another quantity called **branching ratio** can be defined by the definition of the previous ones:

$$\frac{\Gamma(A \longrightarrow f)}{\Gamma_A} = \text{Branching ratio} \tag{2.4}$$

We can now introduce the **cross section**. Let's imagine a fixed target experiment, where a beam of A particles of density n_A and velocity v_A, are shot at the fixed center B. What we can measure includes the rate R at which we see scatterings from the beam:

$$\mathrm{R} = \frac{\text{Number of events}}{\text{Time}} = n_A v_A \sigma_i \tag{2.5}$$

with σ_i the cross section of the process, which has the dimension of an area and it is measured in barn (10^{-28} m^2). It is the effective area that the target B presents to the beam. Another important quantity is the **luminosity**, i.e.:

$$\mathcal{L} = \frac{R}{\sigma_i} \tag{2.6}$$

Returning to the cross section, an alternative definition can be given. Imagine two bunches of particles A and B aimed at one another, namely a collision between two beams. The key idea is that the second beam is the target, so we consider $N_B = n_B l_B A_B$ in order to calculate the rate:

$$R = n_A n_B l_B A_B |v_A - v_B| \sigma_i \tag{2.7}$$

As pointed before, every beam is composed of bunches with the following gaussian distributuion:

$$\frac{\mathrm{d}N}{\mathrm{d}s} = \frac{N}{2\pi\sigma_x\sigma_y} e^{-\left(\frac{x^2}{2\sigma_x^2}+\frac{y^2}{2\sigma_y^2}\right)} \tag{2.8}$$

The number of interations per bunch is $N_{\text{int}} = \sigma_{\text{int}} \frac{N_1 N_2}{4\pi\sigma_x\sigma_y}$ and the bunch frequency is f. Therefore, we can calculate the rate:

$$R_i = N_{\text{int}} f = \sigma_{\text{int}} \frac{N_1 N_2}{4\pi\sigma_x\sigma_y} \tag{2.9}$$

2.2 Partial Width and Cross Section calculation

The partial width and the cross section for a certain process can be calculated through **Fermi's Golden Rule** in a very practical way. By using the time evolution operator T, we can write:

$$\langle 1, 2, \ldots, n | \, T \, | A(p_A) \rangle = \underbrace{\mathcal{M}(A \longrightarrow 1, 2, \ldots, n)}_{\text{Invariant matrix element}} (2\pi)^4 \underbrace{\delta^{(4)}\left(p_A - \sum_{i=1}^{n} p_i\right)}_{E,\vec{\mathbf{p}} \text{ conservation}} \tag{2.10}$$

It is useful to work out the dimension of $\mathcal{M}$. The operator T is dimensionless, and the states have total dimension $\text{GeV}^{-(\text{n}+1)}$. The delta function has units GeV^{-4}. Then the invariant matrix element has the units:

$$\mathcal{M} \sim \text{GeV}^{3-\text{n}} \tag{2.11}$$

Now, to find the total rate, we must integrate over all possible values of the final momenta. This integral is called **phase space** and for n final particles, the expression for the phase space integral is:

$$\int \mathrm{d}\Pi_n = \int \frac{\mathrm{d}^3 p_1}{(2\pi)^3 2E_1} \cdots \frac{\mathrm{d}^3 p_n}{(2\pi)^3 2E_n} (2\pi)^4 \delta^{(4)}\left(p_A - \sum_{i=1}^{n} p_i\right) \tag{2.12}$$

However, we also need to normalize. So the initial state $|A\rangle$ will yield:

$$|A\rangle \longrightarrow \frac{1}{2E_A} \qquad \text{Initial state} \tag{2.13}$$

Finally, the Fermi Golden Rule formula for a partial width to an n-particle final state f is:

$$\Gamma(A \longrightarrow f) = \frac{1}{2M_A} \int \mathrm{d}\Pi_n |\mathcal{M}(A \longrightarrow f)|^2 \tag{2.14}$$

If the final state particles have spin, we need to sum over final spin states. The initial state A is in some state of definite spin. If we have not defined the spin of A carefully, an alternative is to average over all possible spin states of A. By rotational invariance, the decay rate of A can't depend on its spin orientation.
Concerning the cross section, a formula for this quantity is constructed in a similar way. We need the matrix element for a transition from the two initial particles A and B to the final particles through the interaction. So, it reads:

$$\sigma(A+B \longrightarrow f) = \frac{1}{2E_A E_B |v_A - v_B|} \int \mathrm{d}\Pi_n |\mathcal{M}(A+B \longrightarrow f)|^2 \tag{2.15}$$

2.3 Phase Space integral calculation

Phase space plays a very important role in particle physics. The default assumption is that final state particles are distributed according to phase space. This assumption is correct unless the transition matrix element has nontrivial structure. We will procede with a couple of examples/exercises in order to understand the way of working with this kind of computations.

Example 1: Phase space of 2 particles

Most of the reactions we will discuss will have two particles in the final state. So it's better to start with this example. We have to compute:

$$\int \mathrm{d}\Pi_2 = \int \frac{\mathrm{d}^3 p_1}{(2\pi)^3 2E_1} \frac{\mathrm{d}^3 p_2}{(2\pi)^3 2E_2} (2\pi)^4 \delta^{(4)}(p - p_1 - p_2) \tag{2.16}$$

Let's work in the CM system, where $\vec{\mathbf{p}}_1 + \vec{\mathbf{p}}_2 = 0$ and so $\vec{\mathbf{p}}_1 = -\vec{\mathbf{p}}_2$. Hence:

$$P = (E_{\mathrm{CM}}, \vec{\mathbf{0}}) \tag{2.17a}$$
$$p_1 = (E_1, \vec{\mathbf{p}}) \tag{2.17b}$$
$$p_2 = (E_2, -\vec{\mathbf{p}}) \tag{2.17c}$$

We have to integrate over $\vec{\mathbf{p}}_2$ and exploit the properties of δ function:

$$\begin{aligned} \int \mathrm{d}\Pi_2 &= \int \frac{\mathrm{d}^3 p}{(2\pi)^3)} \frac{1}{2E_1 2E_2} (2\pi) \delta(E_{\mathrm{CM}} - E_1 - E_2) \\ &= \int \frac{p^2 \mathrm{d}\Omega}{16\pi^2 E_1 E_2)} \frac{E_1 E_2}{p E_{\mathrm{CM}}} \\ &= \frac{1}{8\pi} \left(\frac{2p}{E_{\mathrm{CM}}} \right) \int \frac{\mathrm{d}\Omega}{4\pi} \end{aligned} \tag{2.18}$$

Example 2: Phase space of 3 particles

It is also possible to reduce the expression for three-body space to a relatively simple formula. Let's work again in the center of mass frame where $\vec{\mathbf{p}}_1 + \vec{\mathbf{p}}_2 + \vec{\mathbf{p}}_3 = 0$ and let the total energy-momentum in this frame be $Q^0 = E_{\mathrm{CM}}$. The three momentum vectors lie in the same plane, called **event plane**. Then the phase space integral can be written as an integral over the orientation of this plane and over the variables:

$$x_1 = \frac{2E_1}{E_{\mathrm{CM}}} \qquad x_2 = \frac{2E_2}{E_{\mathrm{CM}}} \qquad x_3 = \frac{2E_3}{E_{\mathrm{CM}}}$$

which obey the constraint:

$$x_1 + x_2 + x_3 = 2$$

It can be shown that, after integrating over the orientation of the event plane, the integral over three-body phase space can be written as:

$$\int \mathrm{d}\Pi_3 = \frac{E_{\mathrm{CM}}^2}{128\pi^3} \int \mathrm{d}x_1 \mathrm{d}x_2 \tag{2.19}$$

It can be shown, further, that this integral can alternatively be written in terms of the invariant masses of pairs of the three vectors ($m_{12}^2 = (p_1 + p_2)^2$ and $m_{23}^2 = (p_2 + p_3)^2$):

$$\int \mathrm{d}\Pi_3 = \frac{1}{128\pi^3 E_{\mathrm{CM}}^2} \int \mathrm{d}m_{12}^2 \mathrm{d}m_{23}^2 \tag{2.20}$$

This formula leads to an important construction in hadron physics called the **Dalitz plot**.

Example 3: $\pi^+\pi^- \longrightarrow \rho^0 \longrightarrow \pi^+\pi^-$

One important type of structure that one finds in scattering amplitudes is a **resonance**. In ordinary quantum mechanics, a resonance is described by the **Breit-Wigner formula**:

$$\mathcal{M} \sim \frac{1}{E - E_{\mathrm{R}} + \frac{i}{2}\Gamma} \tag{2.21}$$

where E_{R} is the energy of the resonant state and Γ is its decay rate. The Fourier transform of Eq. 2.21 is:

$$\psi(t) = ie^{-iE_{\mathrm{R}}t} e^{-\Gamma\frac{t}{2}} \tag{2.22}$$

Then the probability of maintaining the resonance decays exponentially

$$|\psi(t)|^2 = e^{-\Gamma t} \tag{2.23}$$

corresponding to the lifetime:

$$\tau_{\mathrm{R}} = \frac{1}{\Gamma} \tag{2.24}$$

It is useful to consider a specific example of a resonance in an elementary particle reaction, so we will consider $\pi^+\pi^- \longrightarrow \rho^0 \longrightarrow \pi^+\pi^-$, where the meson ρ^0 is found as a resonance at the ρ^0 mass of 770 MeV. We can represent this process by a diagram of evolution in space-time, as in Figure 2.1.

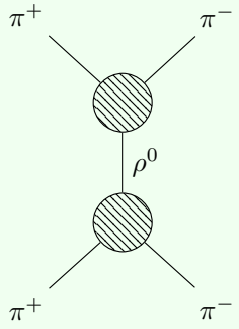

Figure 2.1: Diagram of $\pi^+\pi^- \longrightarrow \rho^0 \longrightarrow \pi^+\pi^-$.

Briefly, what we find is that the final distributions of the invariant masses are not in agreement with what we expect from the phase space distributions for two particles. In this case we can do the calculation in an easy way by studying:

1. $\pi^+\pi^- \longrightarrow \rho^0$ and treat it as a stable particle
2. Using Feynman diagrams.

So, if we consider the cross section of $\pi^+\pi^- \longrightarrow \rho^0$, we get:

$$\sigma(\pi^+\pi^- \to \rho^0) = \frac{1}{4E_A E_B |v_A - v_B|} \int \frac{\mathrm{d}^3 p_C}{(2\pi)^3 2E_C} |\mathcal{M}|^2 (2\pi)^4 \delta^4(p_C - p_A - p_B) \tag{2.25}$$

where $A = \pi^+$, $B = \pi^-$ and $C = \rho^0$. The partial width reads:

$$\Gamma_\rho = \frac{1}{2m_\rho} \int \mathrm{d}\Pi_2 |\mathcal{M}|^2 = \frac{g_\rho^2}{6\pi} \frac{p^3}{m_\rho^2} \tag{2.26}$$

By studying the cross section of the whole process $\pi^+\pi^- \longrightarrow \rho^0 \longrightarrow \pi^+\pi^-$, we get:

$$\sigma(\pi^+\pi^- \longrightarrow \rho^0 \longrightarrow \pi^+\pi^-) = \frac{1}{2m_\rho} \frac{1}{8\pi} \frac{2p}{m_\rho} \int \frac{\mathrm{d}\Omega}{4\pi} \frac{1}{(E_{\mathrm{CM}}^2 - m_p^2)^2 - m_p^2 \Gamma_\rho^2} |k|^2 \tag{2.27}$$

where k is a part related to the spin of ρ^0.
We see a resonance and we are able to fit the data, so we can get the quantities we want to know as the parameters of the best fit.

Chapter 3

Detectors for Particle Physics

Lecture 4.
Monday 18th March, 2019.
Compiled: Friday 27th March, 2020.

3.1 Recap: interaction of particles with matter

The way we identify particles is through their interaction with matter. So, we can detect:

- Charged particles based on ionization, breamsstrahlung, Cherenkov effect.
- γ-rays based on photoelectric/Compton effect and pair production.
- Neutrons based on strong interaction.
- Neutrinos based on weak interaction.

We will give only a phenomenological treatment since the goal is to be able to understand the implications for detector design.

3.1.1 Interactions involving the electrons and heavier particles

Interaction through ionization

A relativistic charged particle with a mass much greater that the mass of the electron, when passing through the matter, is subject to a loss of energy due to the interaction with atomic electrons. These ones can be substracted from the atom and then can be detected. From the total charge collected by the electrodes of a detector, it is possible to know the original interacting particle. The equation that describes this interaction and the loss of energy is the **Bethe-Bloch Equation** (in natural units):

$$-\left\langle \frac{\mathrm{d}E}{\mathrm{d}x} \right\rangle = K\rho \frac{Z}{A}\frac{z^2}{\beta^2}\left[\frac{1}{2}\log\frac{2m_e c^2\beta^2\gamma^2 T_{\max}}{I^2} - \beta^2 - \frac{\delta(\beta\gamma)}{2} - \frac{C}{z}\right] \tag{3.1}$$

where the meaning of the various symbols is given in Table 3.1. A plot showing the stopping power in function of the factor $\beta\gamma$ is given in Figure 3.1. In particular, from this plot we can see some interesting characteristics of the energy loss process. In the first part, the particle loses more energy when the its velocity is slower, so the trend is $\sim \frac{1}{\beta^2}$. When the energy increases, a minimum is met, whose x-axis value is approximately the same for every material. The right part of the plot with respect to this minimum shows a gain in the energy loss which is due to relativistic effects.

Breamsstrahlung energy loss

The Bethe-Bloch formula is valid for particles much heavier than the electron. For this kind of particles, we have that relativistic effects even at low energies, since its mass is lower in comparison with the other particles. So, the electron loses energy through ionization (at lower energies) and **breamsstrahlung**, namely *braking radiation*, when deflected by another charged particle (at higher energies). The different materials that the electron can pass through, are characterized by their **radiation length** X_0,

Symbol	Physical meaning
K	Constant [0.307075 MeVg^{-1}cm^2]
ρ	Density of the absorber
Z	Atomic number of absorber
A	Atomic mass of absorber
z	Atomic number of incident particle
β	Particle velocity in units of c
γ	Relativistic factor derived from β
$T_{\max}$	Maximum energy transfer in a single collision
I	Ionization potential of the absorber

Table 3.1: Bethe-Bloch formula: meaning of all the symbols figuring in its expression.

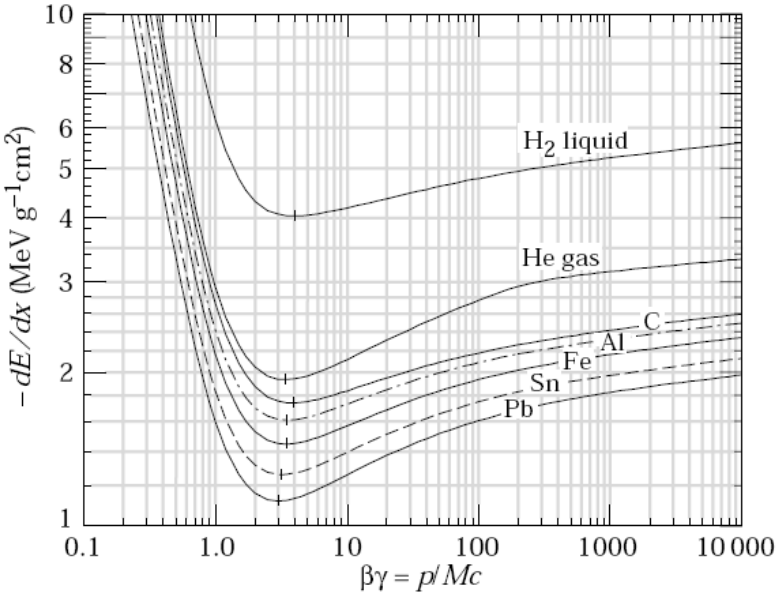

Figure 3.1: Few examples for different materials of Bethe-Bloch formula.

which is a quantity empirically defined as the distance covered by an electron beam before its energy decreases by a factor $\frac{1}{e}$ (63%.). It is measured in g/cm^2 and an approximation of its expression is:

$$X_0 = \frac{A}{4\alpha N_A Z^2 r_e^2 \log \frac{183}{Z^{\frac{1}{3}}}} \tag{3.2}$$

Moreover, there exists a point in which the loss of energy due to ionization and the loss of eergy due to breamsstrahlung are equal. This point is called **critical energy** E_c and a relatively good approximation of its value is:

$$E_c \approx \frac{600 \text{ MeV}}{Z} \tag{3.3}$$

Energy loss as a function of other parameters

Concerning the trend of these losses, we find that the ionization loss decreases logarithmically with E and increases linearly with Z, while bremsstrahlung loss increases approximately linearly with E and it is the dominant process at high energies. This is evident in the plots in Figures 3.2 and 3.3.

3.1.2 Interaction of photon with the matter

Photons can lose energy in several ways. The possibilities are:

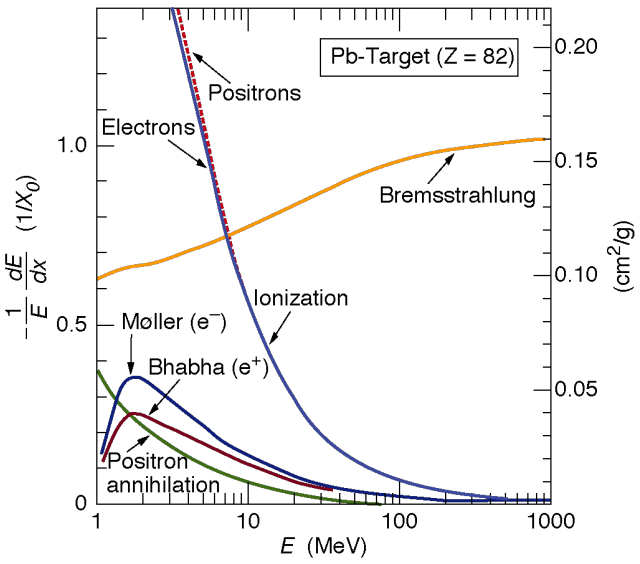

Figure 3.2: Total energy loss for electrons.

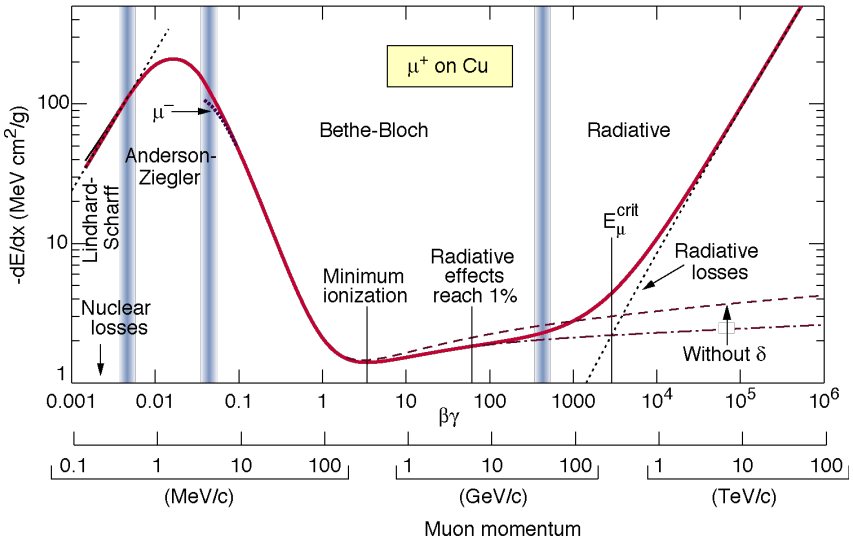

Figure 3.3: Energy loss summary.

- Photoelectric effect on atoms at low energy.
- Compton effect, which is important at medium range energies.
- Pair production, which is the dominant process at higher energies.

It goes without saying that we will focus on pair production, since we are discussing topics whose energies are relatively high. Concerning the cross section of this process, it is approximated by:

$$\sigma_{\text{pair}} = \frac{7}{9}\frac{N_A}{A}\frac{1}{X_0} \tag{3.4}$$

We can characterize a certain material by defining the **attenuation length** λ, namely the length for which the beam of photons inside the material is attenuated by a factor $\frac{1}{e}$, and it is linked to the radiation length by $\lambda = \frac{9}{7}X_0$.

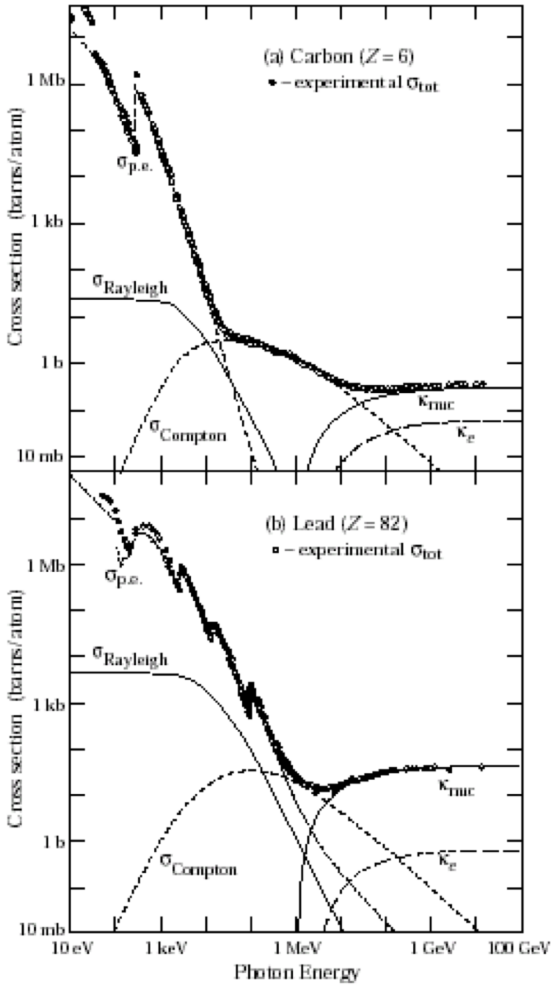

Figure 3.4: Interaction of photons with matter.

3.2 Gaseous, scintillator and solid state detectors

Particles can be identified as point-like objects with a certain mass and some other properties that characterize them. The only way to detect them is to make them interact inside a medium. With this technique we can measure their charge, medium lifetime, velocity, momentum and energy and from these we can retrieve their mass and a lot of other interesting properties. So, let's start a discussion on the many types of detectors that can be employed for a particle experiment.

3.2.1 Gas detectors

These detectors are based on the interaction of the particles with a gaseous medium. The interaction causes the ionization of the atoms in the medium, the charge is collected and from its total amount we can reconstruct the properties of the interacting particles.
In particular, we focus now on the ionization process. When the particle enters in the medium, a first ionization takes place and it is called **primary ionization**. For example, it can be schematized as follows:

$$\text{Particle} + X \longrightarrow X^+ + e^- + \text{Particle} \tag{3.5}$$

The charges produced in the primary ionization interacts as well with the medium

and they create a **secondary ionization**, as follows:

$$X + e^- \longrightarrow X^+ + e^- + e^- \tag{3.6}$$

Experimentally speaking, it is important to evaluate the number of particles produced in the interaction and the relevant parameters to estimate this quantity are the ionization energy E_i, the average energy/ion pair W_i and the average number of ion pairs (per cm) n_T. By putting all together, we get:

$$\langle n_T \rangle = \frac{L \left\langle \frac{\mathrm{d}E}{\mathrm{d}x} \right\rangle}{W_i} \tag{3.7}$$

with L the thickness of the material. Typical values for E_i and n_T are:

$$E_i \sim 30 \text{ eV}$$
$$n_T \sim 100 \ \frac{\text{pairs}}{3 \text{ KeV}}$$

Another important effect to discuss in gas detectors is the **diffusion** in presence of electric and/or magnetic fields. These fields affect the trajectory of the particles transversally and longitudinally. In particular, by measuring the bending of the particle in presence of a magnetic field with a component orthogonal to the velocity vector, we are able to infer the momentum of the particle itself. The electric field influences only the longitudinal diffusion and not the transverse diffusion.

Lastly, another phenomenon that can happen in gas detectors is the **multiplication**. The electrons can undergo to a multiplication process called **Townsend avalanche**. Given the number of electrons at the position x, $n(x) = n_0 e^{\alpha x}$, we have the gain:

$$G = \frac{n(x)}{n_0} = e^{\alpha x} \tag{3.8}$$

where the parameter α can depend on x.
Depending on the gain factor G of the multiplication, four regions of work of the detector can be exploited:

- **Ionization mode**
  The intesity of the electrical field E is low and the electric current at the electrodes of the detector is proportional to the charge produced in primary ionization.

- **Proportional mode**
  It's the region of use for most of detectors and in this case E is sufficiently intense to generate a secondary ionization, so that the initial charge can be multiplied by a certain factor. It's also possible to measure the loss of energy of the original particle, proportional to the collected charge.

- **Limited proportional mode**
  The amplification of ionization charge is now a process that can't be controlled since the electric field is too strong.

- **Geiger mode**
  The electric field is so intense to generate an avalanche of electrons without control, that reaches the electrodes. It is not possible to measure the energy loss in this case, but we can only detect a logic signal that that tells us if a particle has crossed the detector or not.

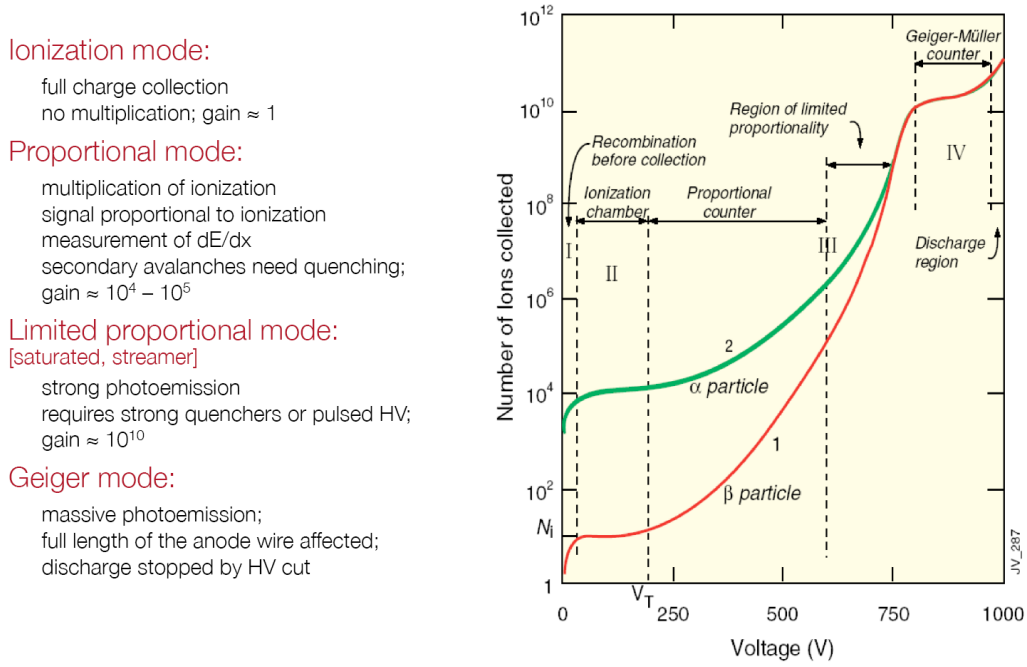

Figure 3.5: Regions of work of ionization detector with a plot giving numeric and practical examples.

3.2.2 Multiwire proportional chambers

They are proportional chambers with multiple wires added to reconstruct the trajectory of the particle. The cathode is the external shell, while the anodes are the internal wires, which generate an electrical field in first order approximation inversely proportional to the distance from the wire.

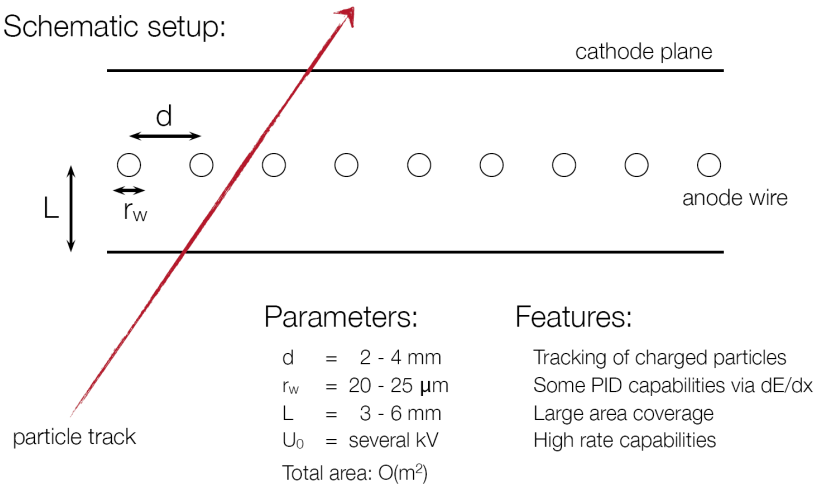

Figure 3.6: Description of multiwire proportional chamber structure and principle of work.

The principle of work is quite simple. The passage of a certain particle produces ionization charges, in particular electrons, which are collected by the nearest wire. Knowing which are all the anodes that collected ionization charge, we can understand the path followed by the crossing particle.

3.2.3 Drift chambers

Drift chambers are very similar to multiwire proportional chambers, however in this case we can have two dimensional informations through time measurments, namely **drift time** measurements.

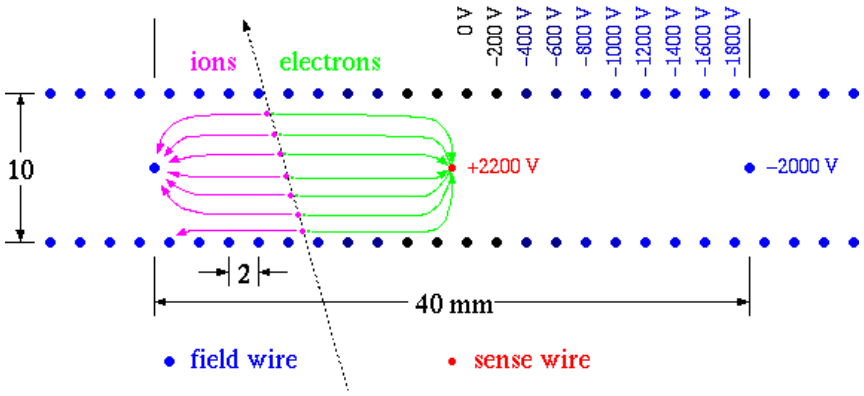

Figure 3.7: Scheme of a drift chamber.

They exploit an external detector such as a scintillator counter, near the chamber, to determine the time t_0 in which the particle arrives. The scintillator detects it and sends a signal to start a sort of chronometer. Then the particle cross the chamber and the electrons from the ionization drift to the nearest anode, captured by the electrical field. At the arrival of the electrons at the anode, a singals is sent to stop the time measurement. Now we have all the informations to extrapolate the drift time t_D, from which we can compute the spatial informations:

$$x = \int_0^{t_D} v_D \mathrm{d}t \tag{3.9}$$

What is important to remember is that the detector is built with a studied geometry in order to get a known drift velocity.

3.2.4 Semiconductor detectors

Semiconductor detectors have the following characteristics:

- High density (respect to gas detectors), so large energy loss in a shorter distance.
- A small diffusion effect, so their position resolution can be less than 10 μm.
- Low ionization energy, so it is easier to produce charged particles when they are crossed.

The materials employed for their construction can vary depending on the purpose of the detector itself. The possibilities are:

- Germanium, which needs to be operated at a very low temperature (77 K) due to small band gap in its microscopic structure.
- Silicon, which can operate at room temperature.
- Diamond, resistent to very hard radiations, with low noise signal. Its employment is still limited by a high cost of natural diamonds, however there exist some techniques through which the artificial production of diamond is a reality. So, diamond detectors are in development up to now.

Silicon detectors are the most common and they are based on a p-n junction with reverse bias applied to enlarge the depletion region. The potential barrier becomes higher so that the diffusion current across the junction is suppressed and the current across the junction is very small ("leakage current").

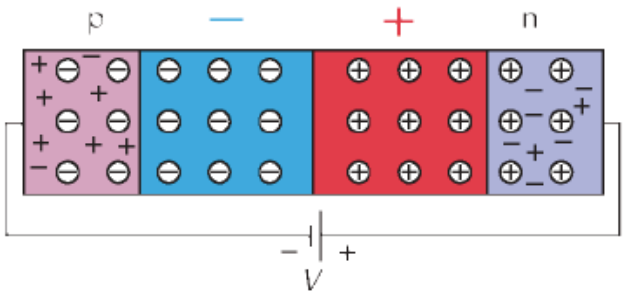

Figure 3.8: A p-n junction with reverse bias applied.

Such a detector can be built in strips. By segmenting the implant we can reconstruct the position of the traversing particle in one dimension. We have a higher field close to the collecting electrodes where most of the signal is induced. Strips can be read with dedicated electronics to minimize the noise.

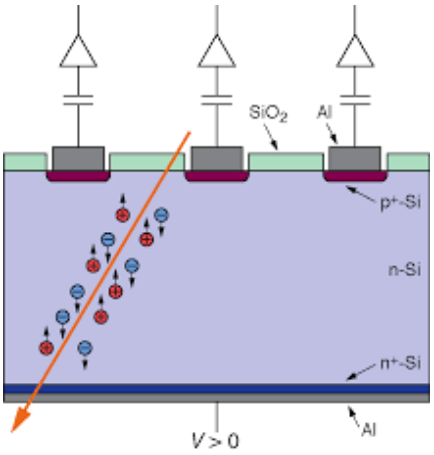

Figure 3.9: Silicon microstrip detector section with representation of ionization charges, generated by a traversing particle.

To have 2-dimensional measurements, double sided silicon detector are used. Moreover, a type of silicon detector still in development is the pixel detector (for 3-dimensional measurements).
Noise contributions can be leakage current and electronics readout. Insted, position resolution is the spread of the reconstructed position minus the true position. For example:

$$\sigma = \frac{\text{pitch length}}{\sqrt{12}} \qquad \text{One strip cluster} \tag{3.10}$$

$$\sigma = \frac{\text{pitch length}}{1.5\frac{S}{N}} \qquad \text{Two strip cluster} \tag{3.11}$$

3.3 Track reconstruction

Track reconstruction is used to determine momentum of charged particles by measuring the bending of a particle trajectory in a magnetic field. The starting point is the

expression of the Lorentz force to which a particle is subjected when moving inside a magnetic field:

$$\vec{\mathbf{F}} = q\vec{\mathbf{v}} \times \vec{\mathbf{B}} \tag{3.12}$$

from which we get:

$$m\frac{v^2}{r} = qvB \Longrightarrow p = rqB \tag{3.13}$$

In fixed target experiments, Eq. 3.13 can be rewritten to:

$$p = qB\frac{L}{\theta} \tag{3.14}$$

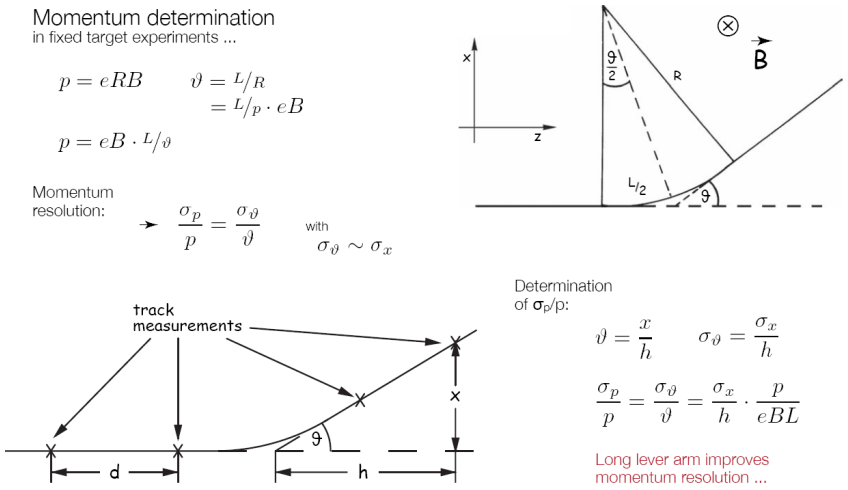

Figure 3.10: Tracking reconstruction example.

3.4 Calorimetry

Lecture 5.
Sunday 24th March, 2019.
Compiled: Friday 27th March, 2020.

Conceptually, a calorimeter is a block of matter, which intercepts the primary particle and is of sufficient thickness to cause it to interact and deposit all its energy inside the detector volume in a subsequent cascade or "shower" of increasingly lower-energy particles. Eventually most of the incident energy is dissipated and appears in the form of heat. Some (usually a very small) fraction of the deposited energy goes into the production of a more practical signal (e.g. scintillation light, Cerenkov light, or ionization charge), which is proportional to the initial energy.
In principle, the uncertainty in the energy measurement is governed by statistical fluctuations in the shower development, and the fractional resolution $\frac{\sigma}{E}$ improves with increasing energy E as $E^{-\frac{1}{2}}$.

Main features of calorimeters

At the outset it was noted that calorimetric detectors offer many other attractive capabilities, aside from the energy response, all of which have since been exploited in varying degrees:

- They are sensitive to charged and neutral particles
- The size of the detector scales logarithmically with the particle energy E, whereas for magnetic spectrometers the size scale with momentum p as $p^{\frac{1}{2}}$, for a given relative momentum resolution $\frac{\Delta p}{p}$.

- Through the use of segmented detectors the information of the shower development allows precise measurements of the position and angle of the incident particle.
- The shower development is a statistical process and the number of secondary particles $\langle N \rangle$ is proportional to the energy E of the incident particle.
- The different response of the materials to electrons, muons and hadrons can be exploited for particle identification.
- Their fast time response allows operation at high particle rates, and the patterns of energy deposition can be used for real-time event selection.

3.4.1 Electromagnetic shower development

The theory of electromagnetic shower development is relatively simple. Electrons and positrons lose energy by ionization and by radiation. The first process dominates at low energy, the second one at high energy. Photons interact either through the photoelectric effect, Compton scattering or pair production. The photoelectric effect dominates at low energies, pair production at high energies. So in our case, for electrons the loss of energy is dominated by bremmstrahlung, for photons by pair production.

E.M. shower model

A simplified electromagnetic shower model in a homogeneous detector has the following assumptions: we assume a material with radiation length of X_0 and we suppose that we have 2^t particles after $t \cdot X_0$ radiation lengths, each with energy $\frac{E}{2^t}$. So the shower stops when $E < E_C$ and the number of particles generated along the path is:

$$N_{\max} = 2^{t_{\max}} = \frac{E_0}{E_C} \tag{3.15}$$

The maximum expansion of the shower is obtained at:

$$t_{\max} \propto \log\left(\frac{E_0}{E_C}\right) \tag{3.16}$$

Molière radius

The lateral development of the shower is described by the **Moliere Radius** ρ_M:

$$R_M \approx (21 \text{ MeV})\frac{X_0}{E_C} \tag{3.17}$$

It is important to note that both X_0 and ρ_M are defined for the asymptotic energy regime (> 1 GeV).
Transversally, the 95% of the energy of shower is contained in a cone of radius $R \sim 2\rho_M$. For lateral shower containment, material differences are much smaller than longitudinally. In addition, there is no energy dependence. A given (sufficiently long) cylinder will thus contain the same fraction of the energy from 1 GeV electromagnetic showers as from 1 TeV ones. Some examples are showed in Figures 3.11 and 3.12.

3.4.2 Hadronic shower development

Nuclear interaction length

Showers generated and developed by hadrons are affected by strong interactions, characterized by the **nuclear interaction length** λ_{int}, namely the average distance hadrons travel before inducing a nuclear interaction. It is expressed in g/cm^2 and for energies up to 100 GeV it scales as:

$$\lambda_{\text{int}} \sim A^{\frac{1}{3}} \tag{3.18}$$

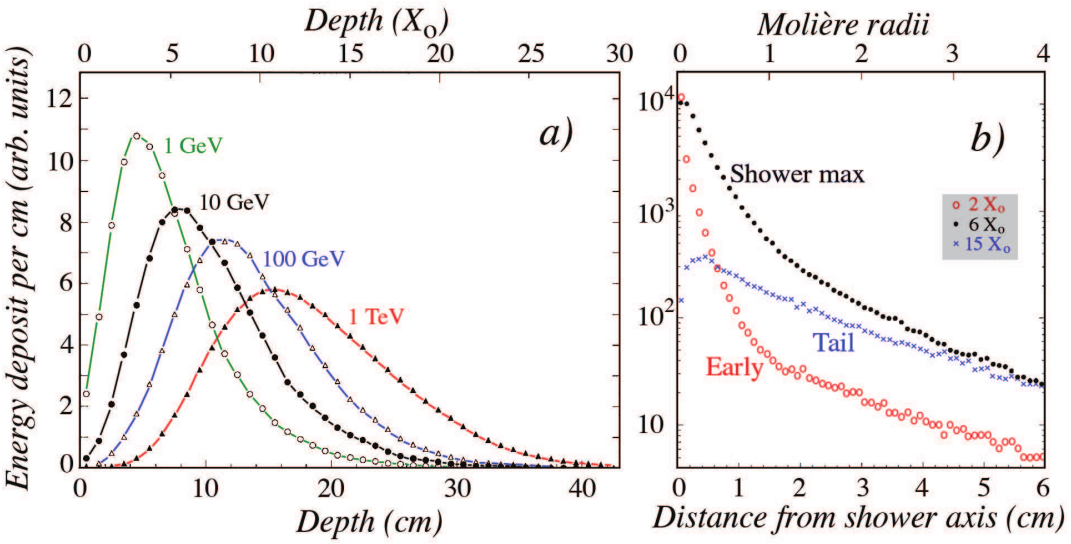

Figure 3.11: Left: the energy deposited as a function of depth for 1, 10, 100 and 1000 GeV electron showers developing in a block of copper; the integral of these curves have been normalized to the same value in order to compare the shower profiles. Right: radial distributions of the energy deposited by 10 GeV electron shower in copper at various depths.

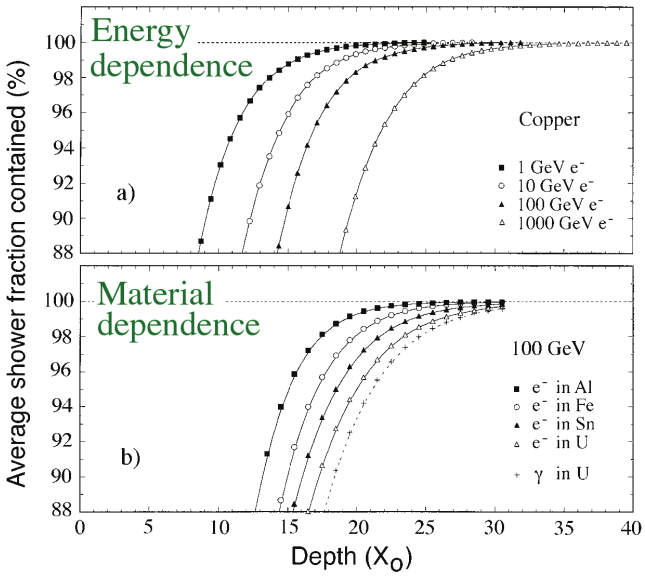

Figure 3.12: Average energy fraction contained in a block of matter with infinite transverse dimensions, as a function of the thickness of the absorber. Up: results for showers induced by by electrons of various energies in a copper absorber. Down: results for 100 GeV electron showers in different absorber materials.

On average, hadronic shower profiles look very similar to the electromagnetic ones, except that the scale factor is usually much larger for the hadronic showers. For example, for copper X_0 amounts to 1.4 cm, while $\lambda_{\text{int}} = 15$ cm.

Effects of strong interactions

Strong interaction is responsible for:

- The production of hadronic shower particles, of which $\sim 90\%$ are pions. The neutral pions decay in 2 γs, which develop an electromagnetic component in the shower. The fraction of this component depends on the energy of the initial particle.
- The occurrence of nuclear reactions. In these processes, neutrons and protons are released from atomic nuclei, however the nuclear binding energy of these

nucleons has to to be provided. Therefore, the fraction of the shower energy needed for this purpose does not contribute to the calorimeter signals. This is the so called **invisible energy** phenomenon.

So we get in function of the distance travelled inside the calorimeter:

$$N(x) = N_0 e^{-\frac{x}{\lambda_{\text{int}}}} \tag{3.19}$$

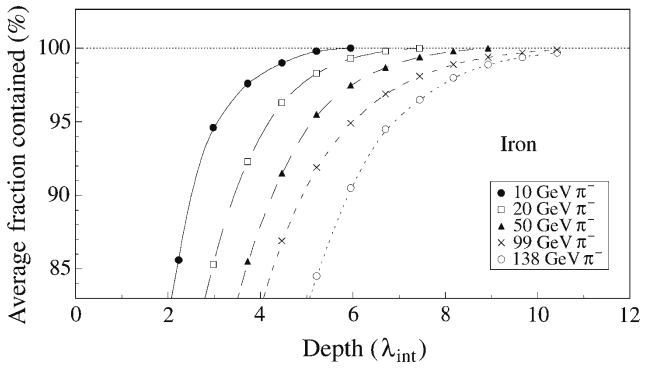

Figure 3.13: Average energy fraction contained in a block of matter with infinite transverse dimensions, as a function of the thickness of the absorber.

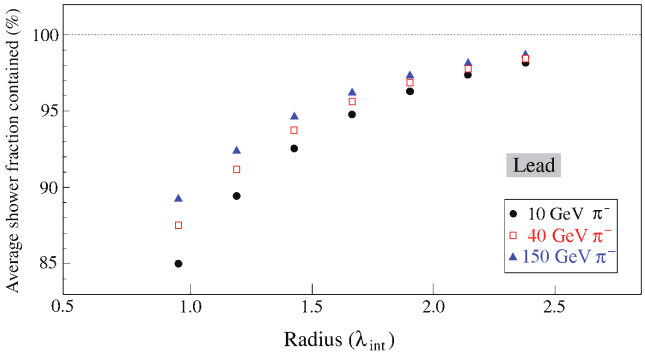

Figure 3.14: Average energy fraction contained in an infinitely long cylinder of absorber material, as a function of the radius of this cylinder, for pions of different energies showering in a lead-based calorimeter.

Consequences od nuclear interaction properties

The large majority of the non-em energy is deposited through nucleons and not through relativistic particles such as pions. These nuclear interaction properties have important consequences for calorimetetry:

- As a result of the invisible energy phenomenon, the calorimeter signals for hadrons are in general smaller than for electrons of the same energy.
- Since the electromagnetic energy fraction is energy dependent, the calorimeter is non-linear for hadron detection.

3.4.3 Classification and response of calorimeters

Calorimeters classification

Calorimeters are distinguished according to their composition into two classes:

- **Homogeneous calorimeters**, in which the absorber and the active (signal producing) medium are one and the same. They are used to get high precision results.

- **Sampling calorimeters**, in which these two roles are played by different media. These are layers of active material and high density absorber. This type of calorimeter is more common.

Calorimeters response

The calorimeter response is defined as the average calorimeter signal per unit of deposited energy. The response is thus expressed in terms of photoelectrons per GeV, pico-coulombs per MeV or something similar. Electromagnetic calorimeters are in general linear, since all the energy carried by the incoming particle is deposited through processes that may generate signals (excitation /ionization of the absorbing medium). Non-linearity is usually an indication of instrumental problems, such as signal saturation or shower leakage. An example of non-linear calorimeter data is given in Figure 3.15.

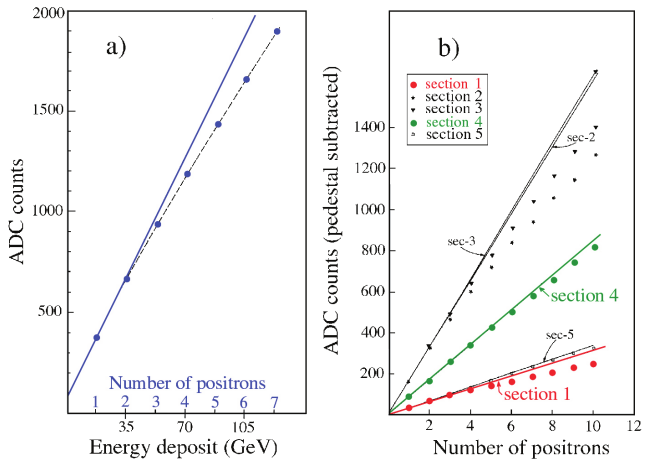

Figure 3.15: Average electromagnetic shower signal from a calorimeter read out with wire chambers operating in the "saturated avalanche" mode, as a function of energy. The calorimeter was longitudinally subdivided.

Fluctuations

Calorimeters are based on physical processes that are inherently statistical in nature, so the precision of calorimetric measurements is determined and limited by fluctuations. We examine here the fluctuations that may affect the energy resolution. Many of them will affect electromagnetic and hadronic calorimeters, but the last one has additional term of uncertainty to be discussed later. Fluctuations and contributions to the energy resolution are:

- Signal quantum fluctuations, such as photoelectron statistics:

$$\frac{\sigma_E}{E} \sim \frac{1}{\sqrt{E}} \tag{3.20}$$

- Shower leakage fluctuations:

$$\frac{\sigma_E}{E} \sim \frac{1}{\sqrt[4]{E}} \tag{3.21}$$

- Fluctuations resulting from instrumental effects, such as electronic noise, light attenuation, structural non-uniformities.

$$\frac{\sigma_E}{E} \sim \frac{1}{E} \tag{3.22}$$

- Sampling fluctuations:

$$\frac{\sigma_E}{E} \sim \text{const} \tag{3.23}$$

So, the calorimeter energy resolution has different contribution from several fluctuation processes, which add in quadrature:

$$\sigma_T^2 = \sigma_1^2 + \sigma_2^2 + \cdots + \sigma_n^2 = \sigma_1 \oplus \sigma_2 \oplus \cdots \oplus \sigma_n \tag{3.24}$$

For electromagnetic showers, the relevant contributions to the energy resolution can be summarized as:

$$\frac{\sigma}{E} = \frac{a}{\sqrt{E}} \oplus b \oplus \frac{c}{E} \tag{3.25}$$

with a the stochastic term (due to intrinsic shower fluctuations, ...), b the constant term, c the noise term.
For hadronic showers, we have some types of fluctuations as in electromagnetic showers, however, there are some additional effects that tend to dominate the performance of hadron calorimeters.

- Fluctuations in visible energy play a role in all hadron calorimeters and form the ultimate limit to the achievable hadronic energy resolution. So this is an irreducible contribution.
- Fluctuations in the electromagnetic shower fraction causes differences between p and π induced showers since in p showers there are no π^0.

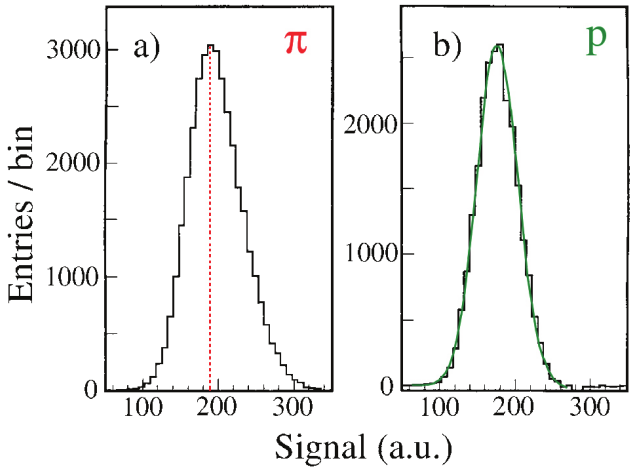

Figure 3.16: Signal distributions for 300 GeV pions and protons detected with a quartz-fiber calorimeter. The curve on the right represents the result of a gaussian fit to the proton distribution.

In the case of hadron calorimeter, the relation used before does not describe the energy resolution due to the two additional effects. For the majority of calorimeters the energy resolution can be approximated by:

$$\frac{\sigma}{E} = \frac{a}{\sqrt{E}} + b \tag{3.26}$$

where a can reach values of 90% and b can be around few %. Therefore, why do we build hadronic calorimeters? In HEP experiments we do not measure single hadrons, we do not reconstruct p, π, etc. We reconstruct jets! Jet reconstruction is complex

TODO

and

3.4.4 Particle identification

TODO

Short lived particles are identified through the resonance. Stable or long lived particles are identified exploiting time of flight, Cerenkov, energy loss, conmbination of tracking and calorimeter.

Chapter 4

Cross section of $e^+e^- \to \mu^+\mu^-$ and $e^+e^- \to hh$

Lecture 6.
Monday 25th March, 2019.
Compiled: Friday 27th March, 2020.

The first is a quantum electromagnetic process and it is relatively simple to compute its cross section at first order. It is also our benchmark when we start to study the second process.

4.1 $e^+e^- \to \mu^+\mu^-$

The idea is now to study the cross section of the first process $e^+e^- \longrightarrow \mu^+\mu^-$. The matrix elements for this process can be constructed by breaking the process down into components. First, the e^+e^- state is annihilated by an electromagnetic current. This current couples to a quantum state of electromagnetic excitation. Finally, this state couples to another current matrix element describing the creation of the muon pair. These passages can be drawn in a Feynman diagram in a very simple way, as in Figure **??**.
The intermediate photon state can be described as a Breit-Wigner resonance at zero mass. Taking the limit of zero resonance mass in the Breit-Wigner formuala, it would then contribute to the scattering amplitude by a factor:

$$\frac{1}{q^2 - m_{\mathrm{R}}^2 + \frac{i}{2} m_{\mathrm{R}} \Gamma_{\mathrm{R}}} \sim \frac{1}{q^2} \tag{4.1}$$

where q is the momentum carried by the photon from the initial to the final state. Moreover, we consider the reaction at energies large compared to the muon mass and, certainly, very far from the mass shell condition $q^2 = 0$ for a photon, therefore we approximate: $m_e = m_\mu = 0$. A resonance contributing to an elementary particle reaction very far from its mass shell is called a **virtual particle**. In this case, we say that the reaction is mediated by a **virtual photon**.
So, the matrix element reads:

$$\mathcal{M}(e^+e^- \longrightarrow \mu^+\mu^-) = (-e) \left\langle \mu^+\mu^- \right| j^\mu \left|0\right\rangle \frac{1}{q^2} (-e) \left\langle 0 \right| j_\mu \left| e^+e^- \right\rangle \tag{4.2}$$

The operator structure $j^\mu j_\mu$ that appears in Eq. 4.2 is called **current-current interaction**.

4.1.1 Properties of massless spin-$\frac{1}{2}$ fermions

We will focus now on the properties of the massless spin-$\frac{1}{2}$ fermions in order to evaluate Eq. 4.2.

The dynamics of fermions and the calculation of matrix elements is quite simplified in the ultrarelativistic limit, which is our case since we are considering energies so large that both the electrons and muons are moving relativistically and their masses can be neglected. In this approximation, the Dirac equation takes the form:

$$i\gamma^\mu \partial_\mu \psi = 0 \tag{4.3}$$

where:

$$\gamma^0 = \begin{pmatrix} 0 & \mathbb{1} \\ \mathbb{1} & 0 \end{pmatrix} \qquad \gamma^i = \begin{pmatrix} 0 & \sigma_i \\ -\sigma_i & 0 \end{pmatrix} \tag{4.4}$$

It is convenient to write this representation by defining $\sigma^\mu = (\mathbb{1}, \vec{\sigma})^\mu$ and $\bar{\sigma}^\mu = (\mathbb{1}, -\vec{\sigma})^\mu$, so:

$$\gamma^\mu = \begin{pmatrix} 0 & \sigma^\mu \\ \bar{\sigma}^\mu & 0 \end{pmatrix} \tag{4.5}$$

Moreover, we will write $\Psi = (\psi_L, \psi_R)$, so the Dirac equation splits into:

$$i\bar{\sigma} \cdot \partial \psi_L = 0 \tag{4.6a}$$
$$i\sigma \cdot \partial \psi_R = 0 \tag{4.6b}$$

At the end of all the calculations, we get the solutions, with the following characteristics[1]:

- $E = p > 0$, $s_3 = \frac{1}{2}$.
- $E = -p < 0$, $s_3 = \frac{1}{2}$.

So we find an electron which is left-handed and a positron which is right-handed, and viceversa, a couple of right-handed electron and left-handed positron.

4.1.2 Matrix element evaluation

The first step is to evaluate the matrix element for $e_R^- e_L^+$ and $e_L^- e_R^+$ annihilations. In all, the process $e^-e^+ \longrightarrow \mu^-\mu^+$ has four amplitudes for the various spin states that are permitted by helicity conservation. All of the differential cross sections have the same structure. So, by considering that:

$$\left|\mathcal{M}(e_R^- e_L^+ \to \mu_R^- \mu_L^+)\right|^2 = \left|\mathcal{M}(e_L^- e_R^+ \to \mu_L^- \mu_R^+)\right|^2 = e^4(1+\cos\theta)^2 \tag{4.7a}$$
$$\left|\mathcal{M}(e_R^- e_L^+ \to \mu_L^- \mu_R^+)\right|^2 = \left|\mathcal{M}(e_L^- e_R^+ \to \mu_R^- \mu_L^+)\right|^2 = e^4(1-\cos\theta)^2 \tag{4.7b}$$

we have for example, for $e_R^- e_L^+ \longrightarrow \mu_R^- \mu_L^+$:

$$\begin{aligned} \sigma &= \frac{1}{2E \cdot 2E \cdot E} \int \mathrm{d}\Pi_2 |\mathcal{M}|^2 \\ &= \frac{1}{2E_{\mathrm{CM}}^2} \frac{1}{8\pi} \int \frac{\mathrm{dcos}\,\theta}{2} e^4 (1+\cos\theta)^2 \end{aligned} \tag{4.8}$$

and for $e_R^- e_L^+ \longrightarrow \mu_L^- \mu_R^+$:

$$\begin{aligned} \sigma &= \frac{1}{2E \cdot 2E \cdot E} \int \mathrm{d}\Pi_2 |\mathcal{M}|^2 \\ &= \frac{1}{2E_{\mathrm{CM}}^2} \frac{1}{8\pi} \int \frac{\mathrm{dcos}\,\theta}{2} e^4 (1-\cos\theta)^2 \end{aligned} \tag{4.9}$$

[1] We can consider the helicity $h = \vec{\mathbf{p}} \cdot \vec{\mathbf{s}}$ to describe the solutions.

With some algebra, we get the differential cross sections:

$$\frac{\mathrm{d}\sigma}{\mathrm{d}\cos\theta} = \frac{\pi\alpha^2}{2E_{\mathrm{CM}}^2}(1+\cos\theta)^2 \qquad \text{for } e_R^- e_L^+ \to \mu_R^- \mu_L^+ \text{ and } e_L^- e_R^+ \to \mu_L^- \mu_R^+ \tag{4.10a}$$

$$\frac{\mathrm{d}\sigma}{\mathrm{d}\cos\theta} = \frac{\pi\alpha^2}{2E_{\mathrm{CM}}^2}(1-\cos\theta)^2 \qquad \text{for } e_R^- e_L^+ \to \mu_L^- \mu_R^+ \text{ and } e_L^- e_R^+ \to \mu_R^- \mu_L^+ \tag{4.10b}$$

At the end, we get the final result:

$$\sigma = \frac{4\pi\alpha^2}{3E_{\mathrm{CM}}^2} \tag{4.11}$$

What is important to remember is that the cross section goes as the inverse squared of the energy in the center of mass. This is a common behaviour for electromagnetic interactions. However, at very high energies this behaviour is broken and there are corrections to consider.
How can we measure muons in a given polarization state? Actually, this is very difficult and it is not possible with the odiern technology, so we can measure an average

Bibliography